Analysis of the singularity avoidance capability of Constant Modulus Algorithms in coherent optical fibre communication systems

Peter A. Nwakamma, Gwillerm Froc, Yves Jaouën, Cédric Ware

Analysis of the singularity avoidance capability of Constant Modulus Algorithms in coherent optical fibre communication systems

Peter Akachi Nwakamma
LTCI, Télécom Paris
Institut Polytechnique de Paris
Palaiseau, France
peter.nwakamma@telecom-paris.fr

Gwillerm Froc
Communication division
Mistubishi-Electric R&D Centre Europe
Rennes, France
g.froc@fr.merce.mee.com

Yves Jaouën
LTCI, Télécom Paris
Institut Polytechnique de Paris
Palaiseau, France
yves.jaouen@telecom-paris.fr

Cédric Ware
LTCI, Télécom Paris
Institut Polytechnique de Paris
Palaiseau, France
cedric.ware@telecom-paris.fr

***Abstract*—Constant Modulus Algorithm (CMA) in dual-polarization optical coherent transmission is revisited for optical access. We introduce a refined CMA, exhibit singularity-free operation up to 5 ps/km$^{0.5}$ polarization mode dispersion in 32GBaud-QPSK system and suggest new ideas.**

***Index Terms*—Constant modulus algorithm, coherent detection, polarization mode dispersion, polarization division multiplexing, optical access**

I. Introduction

The use of multi-dimensional modulation formats such as Quadrature Phase Shift Keying (QPSK) exploiting the possible degrees of freedom of a light wave (i.e. in-phase and quadrature components along two polarization tributaries) and coherent detection optimizes the capacity of optical transmission systems [1]. Recently, this has attracted attention for optical access networks [2], [3]. Moreover, the use of digital signal processing (DSP) alongside coherent detection enables digital equalization of static and dynamic impairments such as chromatic dispersion (CD) and polarization mode dispersion (PMD) respectively by means of digital filters [4]. Dynamic impairments require the use of adaptive equalizers that track the time variation of the channel and update the equalizers' filter coefficients accordingly. A well-known adaptive equalizer is the multiple input multiple output CMA equalizer [5]–[7]. Dealing with optical fibre transmission, the CMA performs polarization demultiplexing while also compensating for PMD [8]–[11]. However, the polarization demultiplexing capability of the CMA is not perfect and the two polarization outputs of the equalizer sometimes converge toward the same input polarization signal, missing the second one. This is the so-called singularity issue of the CMA [8]. Various techniques have been proposed to mitigate this issue as in [12] or specifically in [9] where a constraint against multi-user (MU) correlation is added to the CMA. However, the relationships between the MU-CMA and the channel parameters for singularity avoidance have not been explicitly provided while degrees of freedom that MU-CMA parameters offer have not been fully investigated neither, which we also propose to exploit by introducing amended algorithm: Correlation Avoidance (CA)-CMA. Then, the objective of this paper is to derive and establish these relationships and also analyse the robustness of the algorithms to varying polarization states over a wide PMD range.

In the following, Section II describes the system and the methodology we adopted, Section III introduces the channel model focusing on the PMD and the equalizer. At last, simulations results are presented and discussed in Section IV.

II. System description and methodology

Focusing on the polarization tributaries, the system block diagram that represents the optical coherent system is shown in Fig. 1. A laser in C-band (1550 nm) is split by the polarization beam splitter (PBS) into two orthogonal signals $\mathbf{x}_1$ and $\mathbf{x}_2$

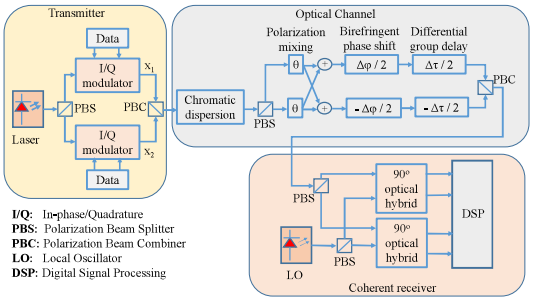

Fig. 1. Block diagram of Dual-polarization optical coherent system

each being modulated by two independent randomly generated data sequences through an in-phase/quadrature (I/Q) modulator. Then, $\mathbf{x}_1$ and $\mathbf{x}_2$ are polarization multiplexed back by the polarization beam combiner (PBC) and propagated through a standard single mode fibre of 20 km length, typical of optical access. The impairments taken into account are the attenuation (0.2 dB/km), the chromatic dispersion (17 ps/nm/km) and PMD. Differently from core or metropolitan networks, optical access networks can suffer from high environmental constraints (*e.g.* aerial fibres) and ageing so the mean PMD can vary over a wide range from link to link and for a given link from time to time. Values ranging from 0.05 ps/$\sqrt{\text{km}}$ up to 1.45 ps/$\sqrt{\text{km}}$ have been reported [13]. Given a Maxwellian probability distribution function for the PMD, an outage probability of 10^{-7} which corresponds to an outage of 3s per year, it leads to realizations of the PMD that can be as high as 8.7 ps/$\sqrt{\text{km}}$. We apply the effects due to attenuation and chromatic dispersion to the polarization division multiplexed (PDM) signal. Then the polarization rotation mixing effects due to birefringent phase shift, and differential group delay are applied to the orthogonal signals after which they are again multiplexed by another PBC. A single birefringent element is considered. This permits analysis of specific polarization states and corner cases that lead to singularities. At the receiver, two PBSs split the PDM received signal and a local oscillator (LO) signal at the same wavelength. These split signals are respectively mixed in two 90° optical hybrids to recover the in-phase and quadrature on both polarization axes. The recovered in-phase and quadrature are then passed on to the digital signal processing (DSP) block. Then, a group velocity dispersion compensation stage mitigates chromatic dispersion. Next, the adaptive fractionally spaced equalizer compensates for the PMD and performs polarization de-multiplexing. Follows carrier phase estimation to mitigate both transmitter and LO phase noise. At last, hard-decision on the transmitted symbols and bit error rate (BER) calculation are performed.

The I/Q transmitted sequences are generated using oversampling ratio of 8, and electronically filtered using Raised Cosine filter balanced at the transmitter and the receiver sides. The I/Q sequences are downsampled to 2 samples per symbol before DSP at the receiver. Additive White Gaussian noise is introduced to achieve typical BER of 10^{-4}.

III. Channel Model

A. PMD Channel Model

With CD already compensated, the remaining PMD is modelled by a unique birefringence element i.e., in the frequency domain as a product of a rotation matrix $\mathbf{R}(\theta)$, a differential group delay (DGD) matrix $\mathbf{DGD}(\tau)$, a birefringent phase shift matrix $\mathbf{B}(\phi)$, and an inverse rotation matrix $\mathbf{R}(-\theta)$:

$$\mathbf{R}(\theta) = \begin{bmatrix} \cos(\theta) & -\sin(\theta) \\ \sin(\theta) & \cos(\theta) \end{bmatrix}, \quad \mathbf{B}(\phi) = \begin{bmatrix} e^{j\phi/2} & 0 \\ 0 & e^{-j\phi/2} \end{bmatrix},$$

$$\mathbf{DGD}(\tau) = \begin{bmatrix} e^{j\omega\tau/2} & 0 \\ 0 & e^{-j\omega\tau/2} \end{bmatrix}, \text{with } j = \sqrt{-1}.$$

The combined channel effect $\mathbf{H_{PMD}}$ can be written as

$$\mathbf{H_{PMD}} = \mathbf{R}(\theta)\mathbf{B}(\phi)\mathbf{DGD}(\tau)\mathbf{R}(-\theta) \tag{1}$$

and the matrix multiplication (1) can be simplified to

$$\begin{bmatrix} \cos(\chi) + j\sin(\chi)\cos(2\theta) & j\sin(\chi)\sin(2\theta) \\ j\sin(\chi)\sin(2\theta) & \cos(\chi) - j\sin(\chi)\cos(2\theta) \end{bmatrix} \tag{2}$$

with $\chi = (\omega\tau + \phi)/2$.

The signal received into the equalizer is impaired by $\mathbf{H_{PMD}}$ and noise $\mathbf{N}(\omega)$ and given, in frequency domain, as

$$\mathbf{Y}(\omega) = \mathbf{H_{PMD}}\mathbf{X}(\omega) + \mathbf{N}(\omega) \tag{3}$$

with $\mathbf{Y}(\omega) = [\mathbf{Y_1}(\omega), \mathbf{Y_2}(\omega)]^T$, $\mathbf{X}(\omega) = [\mathbf{X_1}(\omega), \mathbf{X_2}(\omega)]^T$ and $\mathbf{N}(\omega) = [\mathbf{N_1}(\omega), \mathbf{N_2}(\omega)]^T$.

Resulting time domain expression for the received signal is:

$$\begin{aligned} \mathbf{y_1}(t) &= \mathbf{x_1}(t + \frac{\tau}{2})e^{j\frac{\phi}{2}}\cos^2(\theta) + \mathbf{x_1}(t - \frac{\tau}{2})e^{-j\frac{\phi}{2}}\sin^2(\theta) \\ &+ [(\mathbf{x_2}(t + \frac{\tau}{2})e^{j\frac{\phi}{2}} - \mathbf{x_2}(t - \frac{\tau}{2})e^{-j\frac{\phi}{2}})/2]\sin(2\theta) + \mathbf{n_1}(t) \\ \mathbf{y_2}(t) &= \mathbf{x_2}(t + \frac{\tau}{2})e^{j\frac{\phi}{2}}\sin^2(\theta) + \mathbf{x_2}(t - \frac{\tau}{2})e^{-j\frac{\phi}{2}}\cos^2(\theta) \\ &+ [(\mathbf{x_1}(t + \frac{\tau}{2})e^{j\frac{\phi}{2}} - \mathbf{x_1}(t - \frac{\tau}{2})e^{-j\frac{\phi}{2}})/2]\sin(2\theta) + \mathbf{n_2}(t) \end{aligned} \tag{4}$$

B. CMA, MU-CMA and CA-CMA Equalizers

Focusing on the polarization degree of freedom of the signal, the butterfly structure of the CMA equalizer can be represented as shown in Fig. 2. The vectors $\mathbf{y}_1$ and $\mathbf{y}_2$ denote the fractionally-spaced polarization discrete signals impaired by PMD and noise. They are filtered by four finite impulse response filters (FIR) $\mathbf{f}_{pq}$, $p, q \in \{1, 2\}$ corresponding to four channels resulting from the different polarisation mixing combinations. $\mathbf{f}_{pq}$ FIR are of length L each including fractional spacing. z_1 and z_2 corresponds to the two output polarization signals. Packing the polarization tributaries into vectors and the $\mathbf{f}_{pq}$ into matrix $\mathbf{f}$, one can write at symbol period k, $z(k) = \mathbf{f^T}(k)\mathbf{y}(k)$, its complex conjugate being $\overline{z}(k) = \overline{\mathbf{f^T}}(k)\overline{\mathbf{y}}(k)$.

CMA pertains to gradient descent algorithms that aims at minimizing a cost function $J(\mathbf{f})$ according to $\mathbf{f}$. Denoting $J(\mathbf{f}(k))$ as $J(\mathbf{f}, k)$, the update equation for the FIR coefficients $\mathbf{f}$ is:

$$\mathbf{f}(k+1) = \mathbf{f}(k) - \mu\nabla_{\mathbf{f},\overline{\mathbf{f}}}J(\mathbf{f}, k), \tag{5}$$

where μ is the step-size and $\nabla_{\mathbf{f},\overline{\mathbf{f}}}$ is the operator whose coefficients can be expressed as $2\partial/\partial\overline{\mathbf{f}}$.

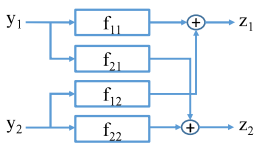

Fig. 2. CMA butterfly equalizer structure

The CMA as proposed by [5] utilizes a cost function $J(\mathbf{f})$ given by (6), which aims at minimizing the expectation of the deviation of the squared modulus of the signal from unity.

$$J_{\text{CMA}}(\mathbf{f}) = \mathbb{E}\left[\left(|z|^2 - 1\right)^2\right] = \mathbb{E}\left[\left(z\overline{z} - 1\right)^2\right] \quad (6)$$

However, in a PDM context, the polarization impairments as PMD induce correlations between the input signals which leads to CMA singularities [8]–[11]. Hence, if these correlations are penalized, the equalizer can be made more robust against singularities. This is the reasoning followed by [9] adding a cross-correlations constraint to $J(\mathbf{f})$ that becomes:

$$J_{\text{MU-CMA}}(\mathbf{f}) = J_{\text{CMA}}(\mathbf{f}) + J_{\text{CA}}(\mathbf{f})$$
$$\text{with } J_{\text{CA}}(\mathbf{f}) = \sum_{p,q;p\neq q} \sum_{\delta=\delta_1}^{\delta_2} |r_{pq}(\delta)|^2, \quad (7)$$

where $r_{pq}(\delta) = \mathbb{E}\left[z_p(k)\overline{z_q}(k-\delta)\right]$ is the expectation of the cross-correlations between equalizer polarization outputs p and q ($p,\ q \in \{1,2\}$) at k, δ being the correlation lag that permits to embrace the maximum DGD. The constraint on the cross-correlations is introduced by their square modulus since otherwise, being either positive or negative they could cancel out each other, thus reducing the strength of the constraint.

The update equations (5) now becomes:

$$\mathbf{f}_{pq}(k+1) = \mathbf{f}_{pq}(k) - 2\mu\left[\frac{\partial J_{\text{CMA}}(\mathbf{f},k)}{\partial \overline{\mathbf{f}}_{pq}} + \frac{\partial J_{\text{CA}}(\mathbf{f},k)}{\partial \overline{\mathbf{f}}_{pq}}\right] \quad (8)$$

with

$$\frac{\partial J_{\text{CMA}}(\mathbf{f},k)}{\partial \overline{\mathbf{f}}_{pq}} = 2\mathbb{E}\left[\left(|z_p(k)|^2 - 1\right) z_p(k)\overline{\mathbf{y}}_q(k)\right] \quad (9)$$

and

$$\frac{\partial J_{\text{CA}}(\mathbf{f},k)}{\partial \overline{\mathbf{f}}_{pq}} = \sum_{\substack{n=1\\n\neq p}}^{2} \sum_{\delta=\delta_1}^{\delta_2} r_{pn}(\delta)\ \mathbb{E}\left[z_n(k-\delta)\ \overline{\mathbf{y}}_p(k)\right]. \quad (10)$$

Plugging (9) and (10) into (8) provides the individual filter tap update equations with both CMA and CA contributions:

$$\mathbf{f}_{pq}(k+1) = \mathbf{f}_{pq}(k) - 2\mu\{2\mathbb{E}\left[\left(|z_p(k)|^2 - 1\right) z_p(k)\overline{\mathbf{y}}_q(k)\right]$$
$$+ \sum_{\substack{n=1\\n\neq p}}^{2} \sum_{\delta=\delta_1}^{\delta_2} \mathbb{E}\left[z_p(k)\overline{z_n}(k-\delta)\right]\ \mathbb{E}\left[z_n(k-\delta)\ \overline{\mathbf{y}}_p(k)\right]\}. \quad (11)$$

Often, $\mathbb{E}[.]$ that applies to the CMA contribution is omitted in the literature. One reason might be that it is not implemented since, as the iteration process progresses, the information from the past samples are propagated into the update equations which mimic an averaging over a sliding window. Thus, without additional complexity, random fluctuations of the channel as the alphabet modulation or the intensity noise are sufficiently filtered out. We have tested this assumption by comparing results obtained with and without an explicit averaging over sliding windows and we have been able to confirm this inference. Hence, we do not account for it either. Conversely, considering the cross-correlation contribution that is PMD dependent, the averaging operation has a deep impact on the proper convergence of the algorithm as shown and discussed in the following of the paper. Thus, here, $\mathbb{E}[.]$ is implemented using a uniform averaging over the most recent w symbols as introduced in (12).

Dealing with the correlation lag δ, the symmetric interplay of the polarizations suggests considering values centered at zero. In that case, the property of the discrete cross-correlation $r_{pq}(\delta) = r_{qp}(-\delta)$ allows to reduce the summation over δ to the positive integers while doubling related cross-correlation contributions. Then, also doubling the contribution at $\delta = 0$ and making $\mu' = 4\mu$ leads to update equations similar to [9]. This is not the way we have followed, implementing strictly the cross-correlation over $[-\delta_2, \delta_2]$.

Finally, comes an original set of coefficients update equations used in the remaining of the paper referred as CA-CMA:

$$\mathbf{f}_{pq}(k+1) = \mathbf{f}_{pq}(k) - 2\mu\{2(|z_p(k)|^2 - 1) z_p(k)\overline{\mathbf{y}}_q(k) + \frac{1}{w^2} \times$$
$$\sum_{\substack{n=1\\n\neq p}}^{2} \sum_{\delta=-\delta_2}^{\delta_2} \sum_{i=k}^{k-w+1} \left[z_p(i)\overline{z_n}(i-\delta)\right] \sum_{i=k}^{k-w+1} \left[z_n(i-\delta)\ \overline{\mathbf{y}}_p(i)\right]\}. \quad (12)$$

IV. Simulation Results

A. Simulation parameters and results

The aim of the simulation is to verify through the analysis of the number of singularities n_s, the capabilities of the CA-CMA algorithm against PMD according to the parameters of the CA-CMA: the number of taps L, the correlation lag δ_2, and the window size, w. To that turn, we subject the CA-CMA algorithm to polarization states and PMD variations as listed in table I. We considered 2000 polarization states uniformly distributed over the Poincaré sphere. Deterministic PMD values range over 0 to 10 ps/$\sqrt{\text{km}}$. In total, this gives 2420 possible combinations of variables. We have considered proper convergence of the algorithms toward the steady state once the relative change in the values of the equalizer tap weights falls down to a given mean absolute error threshold value th.

Fig. 3 shows the singularity signature n_s as a function of the parameter combinations for CA-CMA with th equals 3×10^{-4} and 10^{-5}, and for conventional CMA with th equals to 10^{-5}. The periodic pattern is due to the repeated ordering of the other parameters for the different PMD values which make up the parameter combinations. These combinations are described by the parameter combination index on the X-axis. Related values of the parameters are displayed in the bottom. We observe an overall n_s variation that remains relatively consistent across all parameter combinations up to 4 ps/$\sqrt{\text{km}}$ PMD. Then, it increases to a maximum between parameter combination indices 1500 and 2000 corresponding to 7 and 8 ps/$\sqrt{\text{km}}$ respectively before decreasing toward an average of 50 after 8 ps/$\sqrt{\text{km}}$. Whereas CMA equalizer never achieves singularity-free operation, up to 4 ps/$\sqrt{\text{km}}$ PMD, there are

TABLE I
SIMULATION PARAMETERS

Parameter	Value
Modulation format	QPSK
Baud rate R_s	32 GBd
Oversampling	2 at the equalizer inputs
Fibre length l	20 km
Dispersion parameter	17 ps/nm/km (C-band)
PMD realizations	[0: 10] ps/$\sqrt{\text{km}}$
Theta, θ	$[-\pi/2 : \pi/2]$
Phi, ϕ	$[0 : \pi]$
Bit Error Ratio (BER)	10^{-4}
Number of taps of equalizer L	[5, 9, 13, 17, 21]
Iterations Stopping criterion th	$[3 \times 10^{-4}, 10^{-5}]$
Step-size μ	0.001
Correlation lag δ_2	[0: 10]
Correlation window size w	[10, 20, 30, 40]

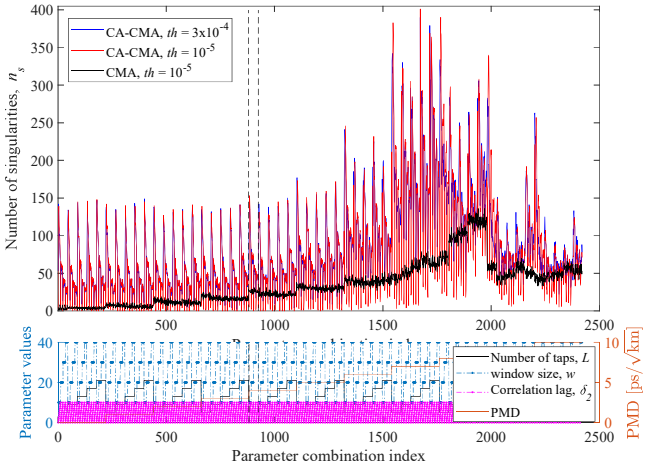

Fig. 3. Singularity signature for CMA, CA-CMA

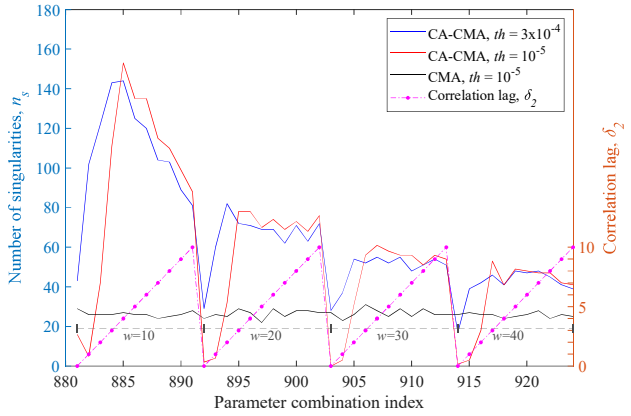

Fig. 4. Singularity signature of CMA and CA-CMA according to w and $\delta 2$ at 4 ps/$\sqrt{\text{km}}$ PMD for 5 filter taps.

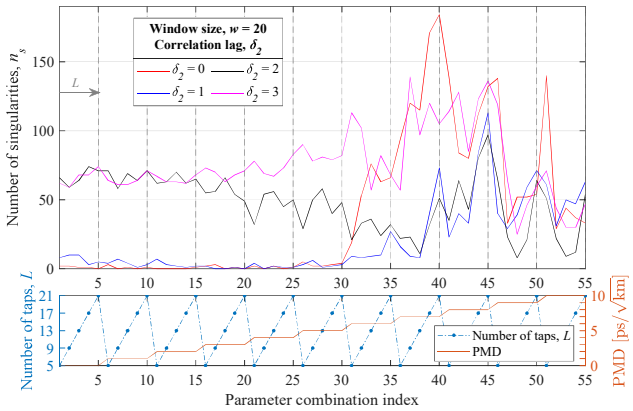

Fig. 5. Dependence of singularities on δ_2 at w = 20 for CA-CMA

sets of parameters that guarantee zero singularities using CA-CMA.

Fig. 4 is a zoom on one spike of Fig. 3, near the parameter combination index 1000 (i.e. 4 ps/$\sqrt{\text{km}}$ PMD) and also retaining only the combination corresponding to $L = 5$. The regions over which the window size w is constant are along the horizontal dashed lines. CA-CMA with th of 3×10^{-4} doesn't achieve zero singularity whereas CA-CMA for th equals to 10^{-5} does. While not shown here, lower th have been tested over the combinations set for both CMA and CA-CMA. It did not provide any further reduction of n_s. Thus, 10^{-5} can be seen as the optimal threshold. Otherwise, Fig. 4 shows that n_s decreases as w increases. However, at each w, two regions can be identified: a dip at the smallest δ_2 (0,1), with few singularities that increasing w can reduce down to zero and another region with high n_s levels on which, increasing w has a stronger quenching impact than increasing δ_2.

So, focusing on δ_2 lowest values, the impact of δ_2 according to PMD and the number of taps is shown Fig. 5, for a given w. For $\delta_2 = 0$, as already underlined, CA-CMA can ensure zero singularity up to 4 ps/$\sqrt{\text{km}}$ at some L. Afterwards, n_s increases sharply. For $\delta_2 = 1$, although robust against singularities at low PMD, from 0 up to 3 ps/$\sqrt{\text{km}}$, zero singularity is not achieved, contrary to the range 3 to 5 ps/$\sqrt{\text{km}}$. After 5 ps/$\sqrt{\text{km}}$, n_s increases sharply . For $\delta_2 = 2$, over 0-2 ps/$\sqrt{\text{km}}$ the curve levels off before decreasing down to a minimum shifted by about 2 ps/$\sqrt{\text{km}}$ as compared to the case $\delta_2 = 1$. Then, it increases again sharply. However, in any case n_s is always significantly higher than what is obtained with δ_2 equals 0 or 1. The curve for $\delta_2 = 3$ has similar behaviour but shifted even further toward the highest PMD values.

Fig. 6 plots the set of parameters leading to zero singularity i.e. the operating points of CA-CMA. From 0 to 5 ps/$\sqrt{\text{km}}$ PMD, the number of taps 13 allows to cover the overall PMD range. Here, can also be found the highest density of working {PMD,w} couples. L equals to 9 and 21 allows to cover PMD up to 4 ps/$\sqrt{\text{km}}$, while with $L = 5$, the algorithm shows weaker avoidance capability. One can view also that as the PMD increases the window size should be increased to get at least one working point. Particularly, a window size of 10 can only achieve zero singularity in the range of 0-1 ps/$\sqrt{\text{km}}$.

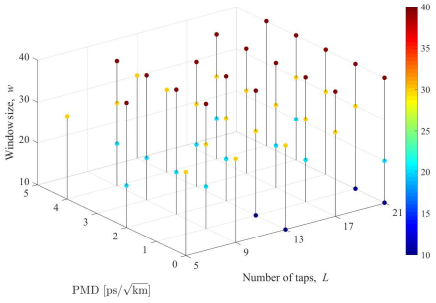

Fig. 6. Parameters leading to singularity-free operation for CA-CMA

B. Discussion

Considering PMD mitigation, as seen in Fig. 3 and Fig. 4, CA-CMA clearly outperforms conventional CMA with respect to the singularity avoidance capability, enabling singularity-free operation. A value of $\delta_2 = 0$ allows zero singularities over 0 to 5 ps/$\sqrt{\text{km}}$ PMD. While in our analysis the PMD is significantly worse than what is usually considered, and although PMD range explored in [9] is not explicitly mentioned, our finding gives a value significantly lower than $\delta_2 = 18$ mentioned in [9]. This lower value would enable a significant reduction of complexity and computation efforts.

Otherwise, as we go deeper into the details, according to Fig. 5, the dips of the singularity signature corresponding to the lowest singularity locations, are dependent on both the value of δ_2 and the PMD. The higher the PMD, the higher the cross-correlation lag should be: δ_2 set to 0 up to 5 ps/$\sqrt{\text{km}}$ PMD, δ_2 set to 1 over the 5 to 6 ps/$\sqrt{\text{km}}$ PMD region, *etc.* 5 ps/$\sqrt{\text{km}}$ PMD corresponds to 22.36 ps time spreading or 71.5% of the symbol time T_s, 5 to 6 ps/$\sqrt{\text{km}}$ corresponds to 71.5% to 86% of T_s, *etc.* Further, Fig. 4, shows that beyond $\delta_2 = 2$ the increase of δ_2 has no impact any more. This is consistent with the fact that at PMD corresponding to DGD less than T_s, the synchronous samples are sufficient to get the cross-correlation and build the constraint. Afterwards, δ_2 equals 1 or 2 is necessary but beyond, since even for a PMD value of 10 ps/$\sqrt{\text{km}}$ the DGD (44.72 ps) is less than 2 symbols, capturing cross-correlation beyond $\delta_2 = 2$ is not relevant.

The issue is that the proper tuning of δ_2 with the PMD does not work as efficiently as the PMD increases: as observed in Fig. 5, even at the minimum of the curves, beyond $\delta_2 = 2$, n_s never reaches the zero-singularity floor any more. However, Fig. 4 reveals that the increase of w is able to quench this increase of n_s, including at its minimum. This gives insight about a relationship between the noise level and the increase of n_s. An interpretation is that increasing the correlation lag δ_2 permits to capture cross-correlations induced with higher DGD but, still, it captures the contributions at lower δ_2 where there is no signal any more. In this context, a refined scheme can be envisioned to extend the capability of CA-CMA by selecting only the cross-correlation in coincidence with the DGD or, in a more general way, giving higher weight to cross-correlations that have higher signal-to-noise ratio (SNR).

V. Conclusion

Analysing the degrees of freedom CMA and MU-CMA offer, we have introduced CA-CMA. Using a deterministic approach, we have then studied the singularity avoidance capability of CA-CMA according to its parameters over a wide PMD realization range. In that respect, more explicitly than what can be found in the literature, we have been able to exhibit the working points that leads to singularity-free operation up to 5 ps/$\sqrt{\text{km}}$ PMD corresponding to DGD up to 22.36 ps in the optical access context. Moreover, the weaknesses of MU-CMA and CA-CMA that prevent covering even wider ranges of PMD have been identified and new ideas have been suggested. Otherwise, as CMA is well suited for constant envelope modulation, we have studied QPSK modulation. Of key interest would be to further consider more advanced modulation formats as Quadrature Amplitude Modulation.

Acknowledgment

The authors do thank Philippe Ciblat and Ghaya Rekaya from Télécom Paris for insightful discussions on theory and methodology.

References

[1] K. Kikuchi, "Fundamentals of Coherent Optical Fiber Communications," *Journal of Lightwave Technology*, vol. 34, no. 1, pp. 157–179, Jan. 2016.
[2] J. Zhang and Z. Jia, "Coherent passive optical networks for 100G/λ-and-beyond fiber access: Recent progress and outlook," *IEEE Network*, vol. 36, no. 2, pp. 116–123, 2022.
[3] V. Houtsma and D. v. Veen, "High speed optical access networks for this decade and the next (invited)," in *2022 IEEE Photonics Conference (IPC)*, 2022, pp. 1–2.
[4] S. J. Savory, "Digital Coherent Optical Receivers: Algorithms and Subsystems," *IEEE Journal of Selected Topics in Quantum Electronics*, vol. 16, no. 5, pp. 1164–1179, Sep. 2010.
[5] D. Godard, "Self-Recovering Equalization and Carrier Tracking in Two-Dimensional Data Communication Systems," *IEEE Transactions on Communications*, vol. 28, no. 11, pp. 1867–1875, Nov. 1980.
[6] Y. Li and Z. Ding, "Global convergence of fractionally spaced godard (cma) adaptive equalizers," *IEEE Transactions on Signal Processing*, vol. 44, no. 4, pp. 818–826, 1996.
[7] C. Papadias and A. Paulraj, "A constant modulus algorithm for multiuser signal separation in presence of delay spread using antenna arrays," *IEEE Signal Processing Letters*, vol. 4, no. 6, pp. 178–181, Jun. 1997.
[8] K. Kikuchi, "Performance analyses of polarization demultiplexing based on constant-modulus algorithm in digital coherent optical receivers," *Optics Express*, vol. 19, no. 10, p. 9868, May 2011.
[9] A. Vgenis, C. S. Petrou, C. B. Papadias, I. Roudas, and L. Raptis, "Nonsingular Constant Modulus Equalizer for PDM-QPSK Coherent Optical Receivers," *IEEE Photonics Technology Letters*, vol. 22, no. 1, pp. 45–47, Jan. 2010.
[10] E. Pincemin, N. Brochier, M. Selmi, O. Z. Chahabi, P. Ciblat, and Y. Jaouen, "Novel Blind Equalizer for Coherent DP-BPSK Transmission Systems: Theory and Experiment," *IEEE Photonics Technology Letters*, vol. 25, no. 18, pp. 1835–1838, Sep. 2013.
[11] J. Xu, Y. Li, X. Hong, J. Qiu, Y. Zuo, H. Guo, and J. Wu, "The performances of singularity-avoidance CMA equalizers in real-time system," *Optics Communications*, vol. 510, p. 127843, 2022.
[12] M. S. Faruk, Y. Mori, C. Zhang, and K. Kikuchi, "Proper polarization demultiplexing in coherent optical receiver using constant modulus algorithm with training mode," in *OECC 2010 Technical Digest*, Jul. 2010, pp. 768–769.
[13] J. Bohata, J. Jaros, S. Pisarik, S. Zvanovec, and M. Komanec, "Long-term polarization mode dispersion evolution and accelerated aging in old optical cables," *IEEE Photonics Technology Letters*, vol. 29, no. 6, pp. 519–522, 2017.